Plasmonic helical nanoantenna as a converter between longitudinal fields and circularly polarized waves

Mengjia Wang,[†] Zhijin Huang,[‡] Roland Salut,[†] Miguel Angel Suarez,[†] Huihui Lu,[*,‡] Nicolas Martin,[†] and Thierry Grosjean[*,†]

[†]*FEMTO-ST Institute UMR 6174, Univ. Bourgogne Franche-Comté, CNRS, France*

[‡]*Guangdong Provincial Key Laboratory of Optical Fiber Sensing and Communications, Department of Optoelectronic Engineering, Jinan University, Guangzhou 510632, China*

E-mail: thuihuilu@jnu.edu.cn; thierry.grosjean@univ-fcomte.fr

Abstract

A wide variety of optical applications and techniques require control of light polarization. So far, the manipulation of light polarization relies on components capable of interchanging two polarization states of the transverse field of a propagating wave (e.g., linear to circular polarizations, and vice versa). Here, we demonstrate that an individual helical nanoantenna is capable of locally converting longitudinally-polarized confined near-fields into a circularly polarized freely propagating wave, and vice versa. To this end, the nanoantenna is coupled to cylindrical surface plasmons bound to the top interface of a thin gold layer. These axis-symmetrical surface waves provide a longitudinal electric picture at focus that is similar to that of a radiating dipole oriented orthogonal to the flat metal surface (parallel to the helix axis). Helices of constant and varying pitch lengths are experimentally investigated. Operating non-resonantly in the traveling-wave regime, constant and varying-pitch helical nanoantennas ensure

a degree of circular polarization of the outcoming light larger than 0.99 over a spectral range of 80 nm and exceeding the 180-nm bandwidth of our laser, respectively. Another consequence is the generation of a directional Gaussian-like beam just after the nanoantenna which keeps its global shape upon propagation. The reciprocal conversion of an incoming circularly wave into diverging cylindrical surface plasmons is demonstrated as well. Interconnecting circularly-polarized optical waves (carrying spin angular momentum) and longitudinal near-fields provides a new degree of freedom in light polarization control.

Introduction

Controlling the polarization vector of light provides a key approach to manipulating light-matter interaction on the nanoscale.[1] In turn, tailoring the local optical response of sub-wavelength structures brings new prospects to light polarization control. Recent advances in plasmonics and metamaterials led to numerous novel polarization systems combining the merits of high compactness, broadband operation and new functionalities.[2–5] So far, polarization control mainly refers to the transverse vector components of a propagating light wave. At small scale however, the 3D nature of light cannot be avoided and a longitudinal optical component arises and can even become dominant for strongly confined fields. This is for instance observed in tightly focused radially-polarized beams[6,7] and surface plasmons tailored by plasmonic lenses,[8,9] tapered tips[10,11] and their variants.[3,12–15] In these cases, the perfect cylindrical symmetry of the near-fields leads to an electromagnetic picture similar to that of a longitudinal radiating dipole (i.e., parallel to the field axis of symmetry). Such longitudinal fields play an important role in super-resolution microscopy,[6,16] fluorescent sensing and imaging,[7,17,18] particle acceleration,[19] laser machining,[20] material processing,[21,22] optical spin-orbit interaction[23–27] and advanced light shaping.[28–30]

Longitudinal electric fields are intrinsic to small scale optics. Therefore, longitudinal-to-transverse field conversion requires the concept of a broadband and directional nanoantenna

to efficiently interconnect near-fields and far-fields[31,32] and fulfill the needs for interconversion between two orthogonal electromagnetic states. Common resonant nanoantennas have a modest ability to tune light polarization and show far-field patterns of low directionality.

Spiral zone plates[33] have shown the ability to convert an incoming circularly polarized propagating light into confined longitudinally-oriented electric fields.[3,15,34–37] The reciprocal configuration has been demonstrated as well.[38] However, besides architectures much larger than the typical size of the light confinements showing dominant longitudinal electric field, which represents limits for small scale applications, their operation suffer from two limits. First, their polarization properties are usually strongly wavelength-dependent. We however note that the chromatism of spiral zone plates can be relaxed using logarithmic-spiral nanoslits of varying width[39,40] or more complex architectures.[41] Second, the light released in free space by a spiral nanoslit needs substantial diffraction to acquire a Gaussian form and propagate self-similarly. This can be an advantage if ones uses these microdevices for light focusing,[36,40] but it may represent a limitation in the design of a polarization optics.

Plasmonic helical nanoantennas have been recently proposed to create and tailor chiroptical effects with direct implication in polarization control.[2,5,42–47] So far, helical nanoantennas were excited with transversely polarized propagating waves. Here, we study the polarization properties of a single plasmonic helix positioned in a nonradiative plasmonic focus showing dominant longitudinal electric field component (perpendicular to the focusing plane,[8,9] parallel to the helix axis). The nano-helix is designed to operate in the traveling-wave regime, also known as the axial-mode in the radiofrequency domain,[48] thereby gaining a directional far-field pattern and a broadband operation.[5] Introducing tapered geometries to the helical structure is a common approach to further enhancing its spectral invariance.[48] As an alternative to nano-helix tapering,[49] we show that varying the pitch length along the helix broadens the operation bandwidth by at least 2.25 times (measurements are limited by our laser bandwidth). The reciprocal process is verified as well, where a circularly polarized incoming optical wave is converted into a tiny light spot of dominant longitudinal electric

field generating an axis-symmetrical diverging surface plasmons all around the nanoantenna. Compared with microscale spiral devices, individual plasmonic helical nanoantennas offer a much smaller footprint together with the prospect of the directional release of a circularly polarized light directly in the form of a Gaussian-like beam.[5] Helical nanoantennas thus provide a new degree of freedom in the control of light polarization at small scale.

Results and discussion

To demonstrate the concept of a converter between longitudinal electric fields and circularly polarized waves, we positioned a helical nanoantenna at the center of a circular slit which perforates a thin gold film on a glass substrate (Fig. 1). The nanoantenna consists of a left-handed four-turn gold-coated carbon helix lying on a 100-nm cylindrical pedestal. First, the skeleton of the subwavelength structure is realized by growing a 105-nm broad carbon wire on a 100-nm thick gold layer with focused ion beam induced deposition (FIBID).[43,50] Two helix configurations, with a varying or constant pitch, are obtained by adjusting the FIBID parameters (see Figs. 1(e) and (f), respectively). The graded pitch length is achieved from the vertical gradients of both precursor concentration and decomposition rate of the FIBID process above the substrate. The resulting helix exhibits average pitch angles of 22.3°, 20.7°, 16.0° and 12.1° from the bottom to the top turn, respectively. The constant-pitch helix (Fig. 1(f)) is obtained by increasing the dwell time by about 30% from the first turn to compensate those gradient effects.[50] We find a homogeneous pitch angle of about 19.5° along the entire structure. The fabricated helical nanostructures are then plasma-sputtered with a 25-nm thick gold layer via a glancing angle deposition technique:[5,44,51,52] the metal target is tilted with an angle of 80° from the helix axis and it is rotated during the deposition time at a constant speed of 2 rev·min^{-1}. Finally, the gold film is milled with a focused ion beam to form a 16-μm diameter and 200-nm wide circular slit surrounding the nanoantenna (see Fig. 1(d)). The helix pedestal coincides with the center of the circular aperture.

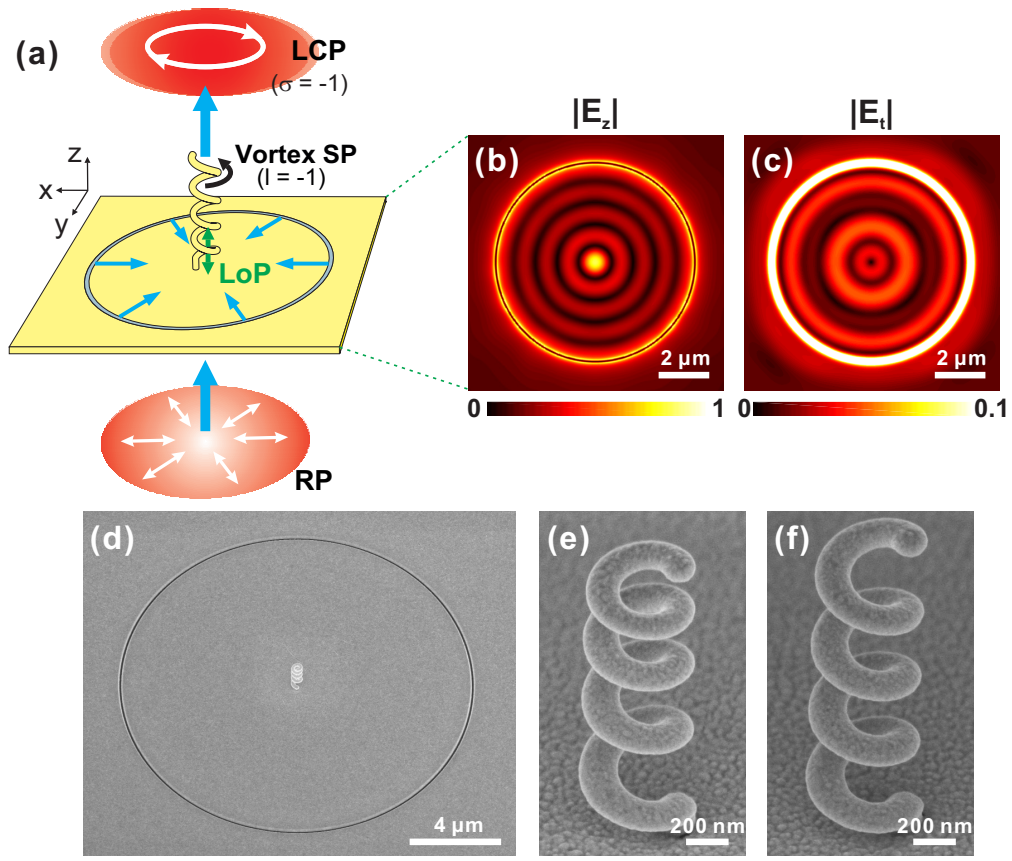

Figure 1: **Plasmonic helical nanoantenna as a subwavelength converter between longitudinal electric fields and circularly polarized light waves**. (a) Schematics of the plasmonic platform used for demonstration: the helix pedestal is set at the center of a circular slit engraved in a thin gold layer. The operation principle of the platform is represented in a conversion from a longitudinal field to circular polarization. The radially polarized incoming beam projected on the back of the sample is converted by the circular slit in plasmonic focused waves. Positioned within the plasmonic focus showing a dominant out-of-plane (longitudinal, with respect to the focusing plane) electric field component (of zero longitudinal angular momentum), the left-handed helical nanoantenna develops vortex surface plasmons of charge l=-1. This twisted plasmon mode is released in free space as left-handed circularly polarized light (σ=-1 per photon) owing to spin-orbit interaction.[53] RP: radial polarization. LCP: left circular polarization. SP: surface plasmons. LoP: out-of-plane/longitudinal field. (b) and (c) Numerically predicted longitudinal ($|E_z|$, out-of-plane) and transverse ($|E_t|$, in-plane) amplitudes of the electric optical field, respectively, plotted 20 nm above a 100-nm thick gold layer engraved with a 7 μm diameter circular slit. The circular slit is illuminated with a radially polarized beam from the substrate. (b) and (c) are normalized to the maximum of the electric field amplitude $\sqrt{|E_t|^2 + |E_z|^2}$. (c) is saturated for a better view of the field pattern within the circular slit. (d) Scanning electron micrograph of a fabricated platform. (e) and (f) Scanning electron micrographs of two plasmonic helices of varying and constant pitch length, respectively.

Upon illumination with a radially polarized beam from the backside, the circular slit launches cylindrical surface plasmons which converge towards the center of the slit.[8] We numerically simulate the electric field distribution of the resulting near-field interference pattern within a circular slit of outer diameter and width equal to 7 μm and 200 nm, respectively. The plasmonic focus at center is defined by an out-of-plane electric field (Fig. 1(b)) surrounded by an in-plane radially-polarized doughnut field of weaker intensity (Fig. 1(c)). The out-of-plane (longitudinal, with respect to the focusing plane) field component (E_z) interferes constructively at the focus whereas the in-plane (transverse, with respect to the focusing plane) field component (E_t) undergoes a destructive interference phenomenon at the center of the circular slit.[8,9] Such a 3D electromagnetic picture is similar to that of an electric dipole oriented along $0z$.[1] Reciprocally, a longitudinally-oriented dipole-like source of light positioned at the center of the circular slit generates axis-symmetrical diverging surface plasmons that are converted back into a radially polarized freely-propagating optical waves by the slit.[11]

The helical nanoantenna is designed to operate in the traveling-wave regime at telecommunication wavelengths.[5] The geometrical requirements on a low-frequency helical antenna to operate in the travelling-wave regime are a circumference that approaches the targeted wavelength and a pitch angle value in between 12° and 14°.[48] With its 505-nm outer diameter, our plasmonic helical nanoantenna satisfies the condition of an outer circumference (of 1.59 μm) matching the targeted telecommunication wavelengths. Optimum polarization conversion has then been numerically found for pitch angles ranging from 10° to 40°. Used as a light-plasmon coupler, the circular slit plays no role in the travelling-wave properties of the plasmonic helix.

In travelling-wave regime, surface plasmons guided along the nanohelix and are released in free space in the form of directional optical waves (see Fig. S1 and Movie S1 in the Supporting Information). The helix can thus be interpreted as a subwavelength chiral waveguide which propagates vortex surface plasmons carrying orbital angular momentum (OAM). The

OAM is imparted to the guided surface plasmons by the chiral nanostructure itself and is thus independent of the excitation conditions. When circular polarization is generated by the helical nanoantenna, its vortex guided mode (of charge ± 1 depending on the helix handedness) is released as freely propagating waves carrying spin angular momentum (SAM) of ± 1 per photon, owing to spin-orbit interaction[5,53] (see Fig. 1(a)). Reciprocally, an impinging circularly-polarized wave excites the twisted mode of the helix for only one polarization handedness,[46] a phenomenon which refers to circular dichroism[54,55] and chiroptical transmission.[2,44,46,47] In the following, we define that a left-handed helical nanoantenna generates a left-handed circular polarization, i.e., the electric field turns counter-clockwise when one looks along the propagation direction of the outcoming wave. Reciprocally, a left-handed plasmonic helical nanoantenna is selectively excited for an incoming left-handed circular polarization.

The concept of a nanohelix as a converter between longitudinal electric fields and circularly polarized waves originates from the ability of low-frequency helical antennas to interconnect circularly polarized freely propagating waves and the fundamental guided mode of a metal wire.[48] Such a subwavelength wire mode has been shown to exist at optical frequencies and to match the longitudinal electric field of a confined light[10,13,56]

To demonstrate the generation of circular polarization from a longitudinal electric light field, we project a focused radially polarized beam onto the back of our sample (Fig. 2(a)). When crossing a rotating LP, such a doughnut beam (Fig. 2(b), left panel) is turned into a two-lobe pattern aligned with the polarizer axis (cf. the four last images on the right of Fig. 2(b)). We then image the overall structure in the far-field with a microscope objective coupled to an infrared camera (cf. Methods). The polarization state of the emerging light is analyzed either with a rotating linear polarizer (LP) or a quarter-wave plate (QWP) followed by a linear polarizer (i.e., a circular analyzer). These polarization analyzers are inserted before the camera. Without analyzer, the image shows an individual spot at the center of a 16-μm diameter narrow light ring (Fig. 2(c), left panel). The ring pattern

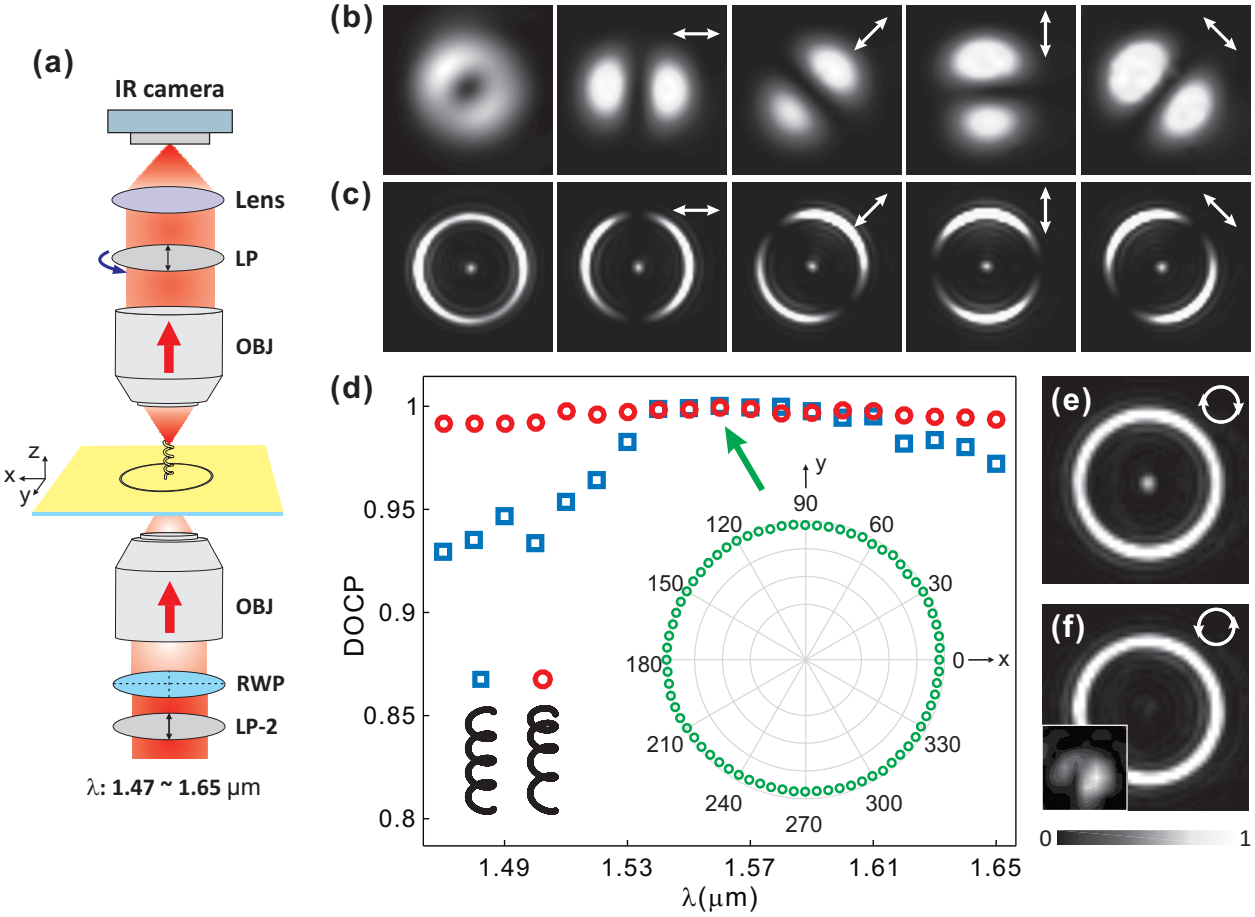

Figure 2: **Conversion of a longitudinal electric field into circular polarization from a fabricated helical nanoantenna**. (a) Schematic diagram of the experimental setup. LP: linear polarizer, OBJ: microscope objective and RWP: radial wave-plate (cf. Methods for details). (b) and (c) Raw and polarization-analyzed optical images at λ=1.56 μm of (b) the incident radially polarized beam and (c) the plasmonic platform in transmission. The white arrows in the figure insets refer to the orientation of the linear polarizer used as a polarization analyzer (called LP). (d) On-axis DOCP spectra of the outcoming optical waves obtained with helical nanoantennas of homogeneous and varying pitches (represented with blue squares and red circles, respectively). Inset: on-axis ellipticity analysis of the output waves at λ= 1.56 μm. (e) and (f) Optical images obtained at λ= 1.56 μm with the varying-pitch helical nanoantenna after inserting (e) a left-handed and (f) a right-handed circular analyzer in front of the camera. The circular analyzer is constituted by a quarter-wave plate followed by a linear polarizer whose axis is at $\pm 45^\circ$ with respect to the waveplate's fast axis. Image size: 25 $\times$ 25 μm^2.

corresponds to the direct transmission of the impinging light through the circular slit. When the rotating LP is inserted, this original circular pattern breaks into two symmetric lobes aligned with the transmission axis of the analyzer (Fig. 2(c), the four last panels on the right), revealing that the light directly outcoupled from the circular slit is radially polarized. The spot located at the center of the bright ring corresponds to the light released by the helical nanoantenna. Since no light is observed in-between the two nanostructures, the distal helix is solely excited with surface plasmons. The optical waves leaving the helix show a constant intensity regardless the LP direction. When the LP is replaced by the circular analyzer, the central spot is visible only when the analyzer selectively transmits left circular polarization (see Figs. 2(e) and (f)). In contrast, when the analyzer selectively transmits the other handedness, a faint doughnut-like pattern is observed (Fig. 2 (f) and inset). This doughnut-like beam is known to be a second-order vortex which originates from angular momentum conservation between the guided mode of a plasmonic structure and freely propagating waves.[15,57] This residual vortex component slightly reduces the helicity of the off-axis outcoming waves. With our fabricated helix, the maximum intensity of this second-order vortex-like field is 0.11 times as high as the overall beam's whereas a ratio of 0.14 is numerically anticipated (cf. Methods and Fig. S2 in the Supporting Information). Owing to its radial polarization, the surrounding light ring remains unchanged for the two handedness of the circular analyzer.

The spectral properties of the helix are investigated by measuring the on-axis degree of circular polarization (DOCP) of the leaving optical waves as a function of the wavelength. The DOCP refers to the distribution of radiated photons prepared in the spin states +1 and −1. Being equal to the absolute value of the normalized stokes parameter S_3/S_0, the DOCP is defined as $|I_{RCP}-I_{LCP}|/(I_{RCP}+I_{LCP})$ where I_{RCP} and I_{LCP} are the intensities of the right and left-handed circularly polarized components of the outcoming light, respectively.[4] Both helical nanoantennas of varying and constant pitch lengths (cf. Figs. 1(e) and (f)) lead to a maximum DOCP value exceeding 0.999 when λ=1.56 μm (Fig. 2(d)). The spectral matching

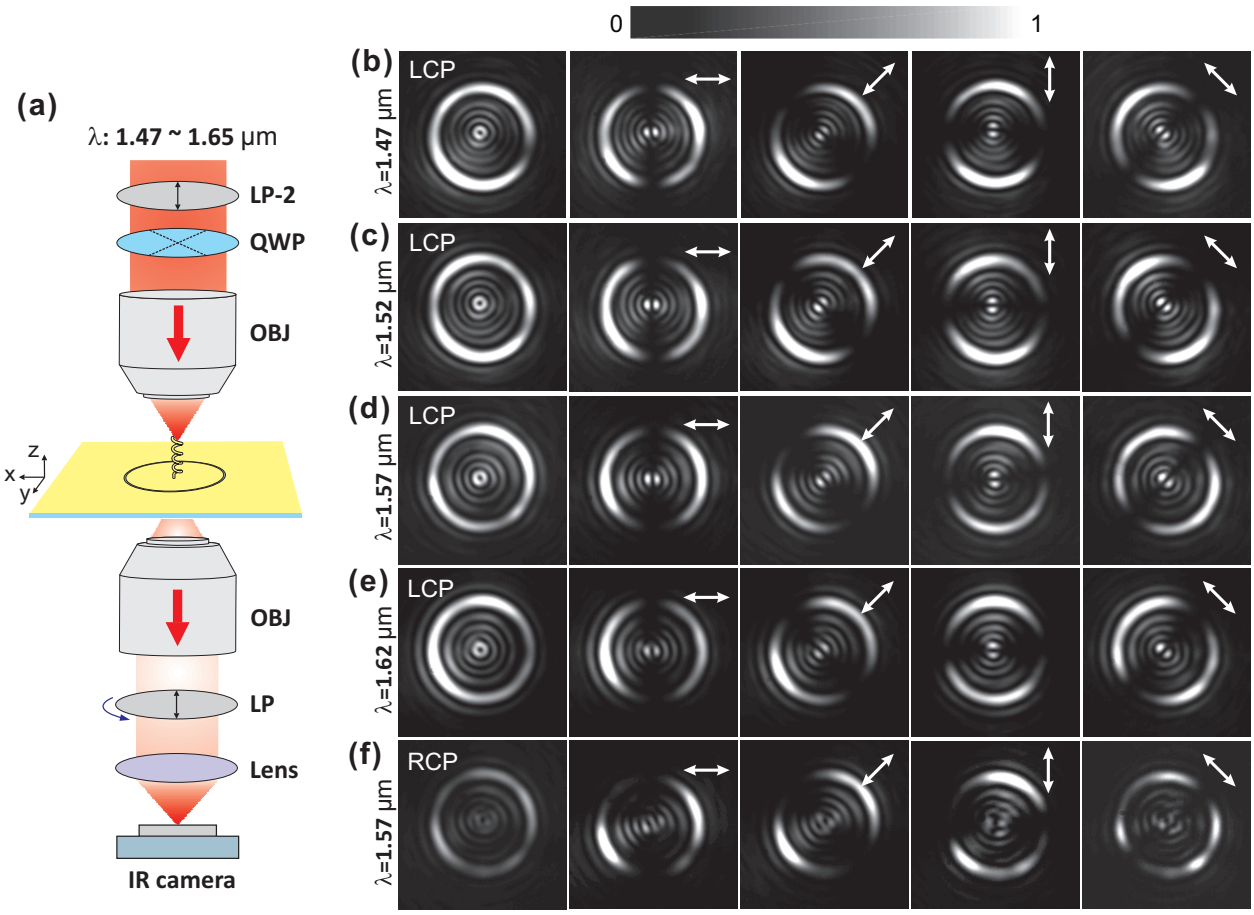

Figure 3: **Conversion from circular polarization to longitudinal electric field**. (a) Schematics of the experimental setup: the left-handed helix is illuminated from the top. LP: linear polarizer. QWP: quarter-wave plate. OBJ: microscope objective. (b–f) Five series of optical images acquired with the varying-pitch helical nanoantenna at wavelengths ranging from 1.47 μm to 1.62 μm by steps of 50 nm. The incoming circular polarization is left-handed in (b–e) and right-handed in (f). (d) and (f) are acquired at the same wavelength of 1.57 μm and with the same camera dynamics. Each series is constituted by a raw optical image (on the left) and four polarization-analyzed images obtained when a linear polarizer is positioned in front of the camera. Four orientations of the linear polarizer, represented with white arrows in the figures, are considered. Intensity attenuation in the polarization-analyzed images (induced by the presence of a polarizer in front the camera) is numerically compensated. Image size: 25 × 25 μm^2.

of the two DOCP maxima would suggest that the spectral condition for a conversion from longitudinal electric field to circular polarization mainly scales with the helix radius, which appears to be consistent with the design rules for radiofrequency helical antennas.[48] For the helix of a constant pitch (Fig. 1(f)), the DOCP remains larger than 0.99 within a wavelength range of 80 nm. Although the plasmonic helix operates in the nonresonant traveling-wave regime,[5,46] its periodic nature limits its spectral bandwidth by providing a wavelength-dependent operation. By breaking the helix periodicity, i.e., by using the varying-pitch helix (Fig. 1(e)), we extend the spectral invariance of the nanoantenna to a broader wavelength range exceeding the 180-nm bandwidth of our laser.

By combining our experimental measurements to the theoretical prediction of the optical properties of a nanoslit (see Section S1 of the Supporting Information), we estimate that the efficiency with which the constant and varying-pitch helices convert incoming surface plasmons into freely propagating waves is of 26.5% and 23.7%, respectively. Such values represent a lower limit of the helix's efficiency as the fabricated nanoslit is expected to be less efficient in converting light into surface plasmons than its theoretical model. Current nanofabrication facilities do not ensure nanoscale slits with perfectly parallel edges and sharp corners.

In a reciprocal approach, a circularly polarized focused wave is projected onto the varying-pitch helix and the back of the sample is imaged with a high numerical aperture microscope objective coupled to an infrared camera (Fig. 3(a); cf. Methods). Figures 3(b) – (e) present four series of five optical images for incoming left-handed circular polarization. Each image series is measured at a wavelength written on the left of the figure. As in Figs. 2(b) and (c), the first panel on the left is a direct image of the structure. The four other panels on the right are acquired in the presence of a LP positioned before the camera, whose orientation is represented with a white arrow. Regardless of the wavelength, the far-field diffraction pattern projected onto the camera is constituted by a bright ring which surrounds a set of concentric circular fringes of lower intensity. Such an optical pattern, which arises from light

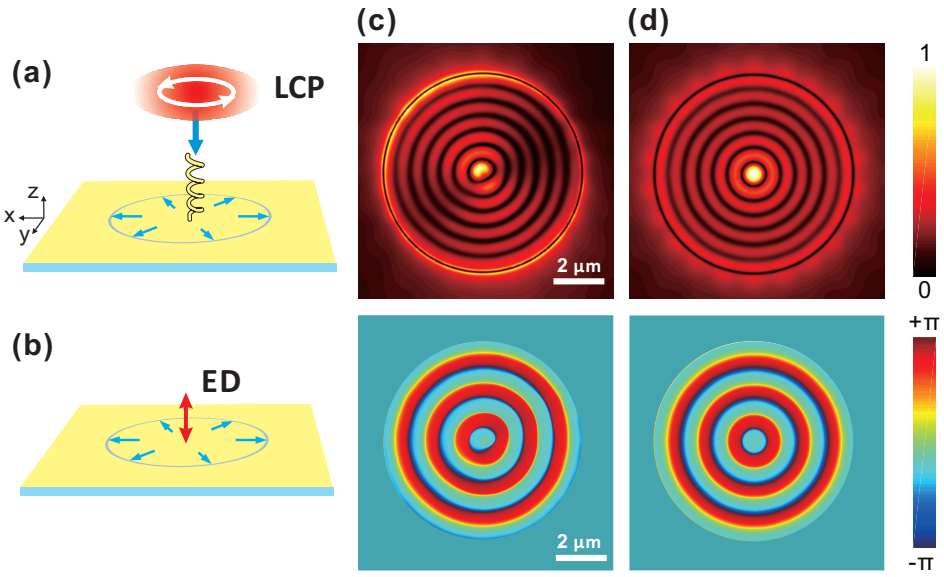

Figure 4: **The helical nanoantenna converts from circular polarization to longitudinal electric field**. (a,b) Schematics of the diverging surface plasmons (blue arrows) excited (a) from a left-handed helical nanoantenna upon illumination with left circular polarization (LCP), and (b), from an (longitudinal) electric dipole oriented perpendicular to the top surface of the metal film (ED). (c,d) Simulated amplitude (upper panel) and phase (downer panel) of the longitudinal electric component (E_z) of the surface plasmons generated at the metal-glass interface by the circular slit, upon the excitation conditions of (a) and (b), respectively. The E_z component is plotted 20 nm beneath the metal-glass interface. The modeled helix has a constant pitch length. The computation parameters are detailed in the Method section.

diffraction by the slit, can be also found at the output of spiral-shaped structures.[40] When a LP is inserted before the camera, the original circular pattern in the images is turned into a two-lobe distribution aligned with the LP axis, which reveals a radial polarization state of the outcoming waves. Such an axially-symmetric optical field at the structure output originates from an isotropic longitudinally-oriented dipole source of surface plasmons at the center of the circular slit (i.e., at the position of the helix). When the helicity of the incident light is flipped, the intensity of the output optical pattern decreases by 2.8 times and the outcoming light loses its radial polarization state (see Figs. 3(f)). The residual optical pattern originates from a direct transmission of the incident light through the slit. The chiral optical response shown in Figs. 3 (d) and (f) evidences the central role of the helix in the light transmission process since the rest part of the plasmonic platform is achiral. The conversion from circular polarization to longitudinal electric field occurs when the incoming polarization handedness is identical to the helix's, which agrees well with past experimental observations on helical plasmonic nanoantennas.[2,46] Fig. 3 thus shows the ability of helical nanoantennas to convert circular polarization in the far-field into a longitudinal electric field in the near-field over the 180-nm spectral bandwidth of our laser. This broadband operation is consistent with that shown in Fig. 2.

Upon illumination with left circular polarization, a left-handed helix excites diverging cylindrical surface plasmons at the metal-air interface (Fig. 4(a)). As they hit the circular slit, these surface waves are converted into radially polarized freely propagating waves together with focused surface plasmons on the opposite metal-substrate interface. We observe in Fig. 4 (c) the longitudinal electric component E_z of these transmitted surface plasmons (in amplitude and phase) plotted 20 nm beneath the metal layer. The phase is selectively represented within the circular slit. Due to computation limitations, the circular slit is shrinked to a diameter of 7 μm. The transmitted longitudinal near-field within the circular slit is constituted by concentric fringes of constant phase, which evidence a near aberration-free plasmonic focusing on the backside of the metal layer. Similar transmitted plasmonic

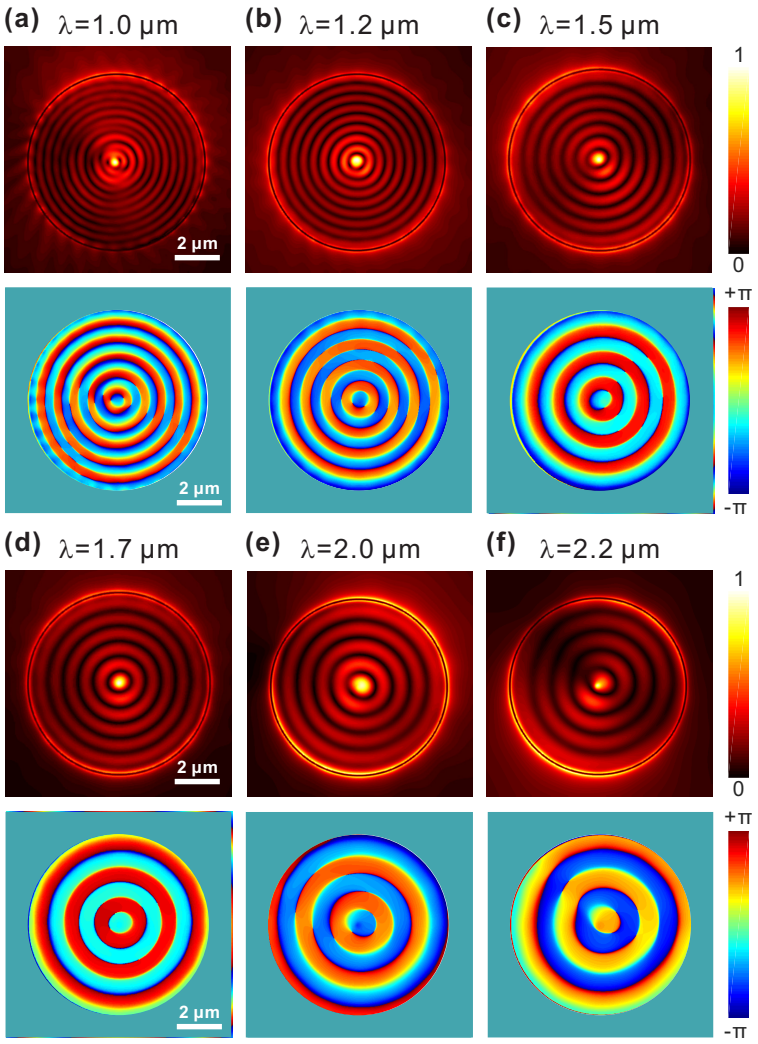

Figure 5: **Broadband conversion from circular polarization to longitudinal electric field**. Simulated amplitude (upper panel) and phase (downer panel) of the longitudinal electric field E_z of the transmitted surface plasmons at the gold-glass interface, with the setup shown in Fig. 4(a). These near-fields are plotted 20 nm beneath the substrate-metal interface and at various wavelengths ranging from 1.0 to 2.2 μm. The modelled helix has a constant pitch length.

field is obtained when the circular slit is excited with a longitudinal electric dipole (i.e., oriented along $0z$) positioned just above the slit center (see Fig. 4(d)). The good agreement between the two electromagnetic pictures of Figs. 4(c) and (d) suggests that upon excitation with left circular polarization, a left-handed helix behaves as a longitudinally-oriented dipole source (i.e., parallel to $0z$) of surface plasmons. We thus numerically confirm that the helical nanoantenna converts impinging circularly-polarized propagating waves into longitudinally-oriented optical near-fields generating axis-symmetrical cylindrical surface plasmons. In this reciprocal approach, the helical nanoantenna absorbs the angular momentum from the impinging light to generate twist-free axis-symmetrical near-fields. We predict that the above-described effect pertains in the 1.2 μm to 2.0 μm wavelength range (see Fig. 5). Such a broadband operation is attributed to the waveguide mode nature of the surface plasmons travelling along the helical nanoantenna. According to Fig. 2(d), a broader operation bandwidth could be expected with a varying-pitch helical nanoantenna.

Conclusion

We demonstrate an individual helical nanoantenna to convert between the circular polarization of a freely propagating wave and longitudinal electric fields in the near-field, thus providing a new degree of freedom in light polarization control. When positioned in the longitudinally-polarized focus of converging surface plasmons, an individual helical nanoantenna is shown to radiate circularly-polarized light that is directly shaped into a Gaussian beam. Reciprocally, upon illumination with circular polarization, the plasmonic helix generates localized longitudinal near-fields which excites axis-symmetrical diverging surface plasmons on a thin metal film. Being non-resonant, the helical nanoantenna operates over a broad spectral range, which is shown to be further widened by breaking the helix periodicity (as an alternative to the well-known tapered helices). Moreover, our fabricated nanoantennas show excellent stability in time during acquisitions as well as unchanged optical performances

even three years after their fabrication. As a new broadband and subwavelength polarization optics, individual plasmonic helices hold promise for applications such as optical information processing, polarimetry, miniaturized displays, optomagnetic data storage, microscopy, sensing and communications. As an example, plasmonic helices may couple longitudinally oriented quantum emitters to right- and left-handed single photons, thus paving the way towards new architectures in polarization-encoded optics and spin-encoded photon qubits with applications in quantum information and opto-spintronics.

Methods

To examine the optical response of the fabricated helices, our experimental setup is built onto a Nikon TE2000 inverted microscope. In the experimental characterization of Fig. 2, a near-infrared light (λ=1.47 – 1.65 μm) emerging from a tunable laser (Yanista Tunics-T100S) is coupled to a single-mode polarization-maintaining fiber (P3-1500PM-FC-2, Thorlabs) and collimated with an achromatic fiber collimator (RC08APC-P01, Thorlabs). The output beam passes successively through an achromatic linear polarizer (LPNIR100-MP2, Thorlabs) and a space-variant half-wave plate (WPV10L-1550, Thorlabs) to produce radially polarized light. The resulting doughnut beam is then focused onto the gold layer with a (4x, 0.1) microscope objective from the backside. A piezo stage (Mad city labs) is used to align the circular slit regarding the focused beam. The sample is imaged in transmission mode with a microscope objective (Leitz Wetzlar NPL FL 63x, 0.9) coupled to an infrared camera (GoldEye model G-033, Allied Vision Technologies GmbH). A proper field lens is inserted before the camera. To investigate the polarization state of the transmitted light, two different analyzers are positioned in between the objective and the field lens. These analyzers are either a rotating linear polarizer (LPNIR100-MP, Thorlabs) or the same fixed linear polarizer with a rotating quarter-wave plate (AHWP05M-1600, Thorlabs) inserted in front. In the reciprocal configuration shown in Fig. 3, the illumination and collection benches are inverted. The

collimated laser beam passes through the circular polarizer and it is then focused onto the helix with the (63x, 0.9) microscope objective. The light transmitted back in the substrate is detected with the (25x, 0.4) microscope objective coupled to the infrared camera. The polarization state of the outcoming light is analyzed with the rotating linear polarizer. In order to compare the transmission intensities regarding two opposite incident handedness, the raw optical images (Figs. 3(d) and (f), left panels) are integrated over the circular area enclosed by the slit boundary.

All the numerical simulations are carried out using the 3D Finite Difference Time Domain (FDTD) method available on a commercial software from Synopsis. The plasmonic core-shell nanowire forming the helical nanoantenna is modeled as a 105-nm diameter carbon cylinder covered with a 25-nm thick gold layer. Such a wire is wound up in the form of a 4-turn helix and is also used to terminate the structure on one end with a 100-nm long pedestal lying on a 100-nm thick gold layer covering a glass substrate. To numerically verify the polarization conversion principle of our nanoantennas, the simpler constant-pitch configuration of the helix is consistently considered. The resulting helical nanoantenna has an outer diameter of 505 nm and a total height of 1.66 μm, which corresponds to a homogeneous pitch angle of approximately 20.7°. The cylindrical pedestal is located at the the center of the 200 nm wide circular slit of a 7 μm diameter that surrounds the nanoantenna. Due to computation limits, the modeled circular slit has a shorter diameter than its experimental counterpart. For the illumination from the substrate, a radially polarized beam is projected onto the circular slit at normal incidence. The beam waist is 8 μm wide, align with the symmetry axis of the circular slit and located 350 nm away from the metal-glass interface. In the reciprocal case, the helix is illuminated from the top with a circularly polarized Gaussian beam whose 1.5-μm waist is aligned with the helix axis and set at a distance of 0 nm from the summit of the nanostructure. The non-uniform grid resolution varies from 30 nm for portions at the periphery of the simulation to 5 nm within and near the helix and the circular slit.

All field simulations are conducted in the continuous wave regime at various wavelengths ranging from 1 μm to 2.2 μm. The total computation volume spans 10 μm in the x and y directions. It extends 1.5 μm below the gold layer in the glass substrate and terminates 4 μm beyond the top of the helix in air. The field distributions shown in Figs. 1(c) and (d) are calculated without the helical nanoantenna and with an illumination from the substrate (incoming radial polarization). Being of shorter diameter than its experimental counterpart, the modelled circular slit over-adds a stronger background to the optical signal from the helix. In that context, the results shown in Figs. 4(d) and 5 are obtained by subtracting the simulated fields with the helix from those anticipated without the nanoantenna to filter out the background signal from the slit.

Acknowledgement

The authors are indebted to Katja Höflich for helpfull discussions. This work is funded by the EIPHI Graduate School (contract ANR-17-EURE-0002), the Region Bourgogne Franche-Comte, the French Agency of Research (contract ANR-18-CE42-0016), the I-SITE BFC (contract ANR-15-IDEX-0003). It is supported by the French RENATECH network and its FEMTO-ST technological facility.

Supporting Information Available

Numerical analysis of the helicity of the optical waves released by an individual helical nanoantenna positioned within a plasmonic focus. Numerical analysis of the operation principle of the plasmonic helix, evidencing a travelling wave regime. Estimation of the efficiencies with which the constant and varying-pitch helical nanoantennas convert longitudinal fields from confined surface plasmons into circularly polarized freely propagating waves.

References

(1) Novotny, L.; Hecht, B. *Principles of nano-optics*, 2nd ed.; Cambridge University Press: New York, 2012; p 564.

(2) Gansel, J. K.; Thiel, M.; Rill, M. S.; Decker, M.; Bade, K.; Saile, V.; von Freymann, G.; Linden, S.; Wegener, M. Gold helix photonic metamaterial as broadband circular polarizer. *Science* **2009**, *325*, 1513–1515.

(3) Chen, W.; Abeysinghe, D. C.; Nelson, R. L.; Zhan, Q. Experimental confirmation of miniature spiral plasmonic lens as a circular polarization analyzer. *Nano Lett.* **2010**, *10*, 2075–2079.

(4) Yu, N.; Aieta, F.; Genevet, P.; Kats, M. A.; Gaburro, Z.; Capasso, F. A broadband, background-free quarter wave plate based on plasmonic metasurfaces. *Nano Lett* **2012**, *12*, 6328–6333.

(5) Wang, M.; Salut, R.; Lu, H.; Suarez, M.-A.; Martin, N.; Grosjean, T. Subwavelength polarization optics via individual and coupled helical traveling-wave nanoantennas. *Light Sci. Appl.* **2019**, *8*, 76.

(6) Quabis, S.; Dorn, R.; Eberler, M.; Glöckl, O.; Leuchs, G. Focusing light to a tighter spot. *Opt. Commun.* **2000**, *179*, 1–7.

(7) Novotny, L.; Beversluis, M. R.; Youngworth, K. S.; Brown, T. G. Longitudinal field modes probed by single molecules. *Phys. Rev. Lett.* **2001**, *86*, 5251.

(8) Lerman, G. M.; Yanai, A.; Levy, U. Demonstration of nanofocusing by the use of plasmonic lens illuminated with radially polarized light. *Nano Lett.* **2009**, *9*, 2139–2143.

(9) Chen, W.; Abeysinghe, D. C.; Nelson, R. L.; Zhan, Q. Plasmonic lens made of multiple

concentric metallic rings under radially polarized illumination. *Nano Lett.* **2009**, *9*, 4320–4325.

(10) Stockman, M. I. Nanofocusing of optical energy in tapered plasmonic waveguides. *Phys. Rev. Lett.* **2004**, *93*, 1–4.

(11) Tugchin, B. N. et al. Plasmonic tip based on excitation of radially polarized conical surface plasmon polariton for detecting longitudinal and transversal fields. *ACS Photonics* **2015**, *2*, 1468–1475.

(12) Janunts, N. A.; Baghdasaryan, K. S.; Nerkararyan, K. V.; Hecht, B. Excitation and superfocusing of surface plasmon polaritons on a silver-coated optical fiber tip. *Opt. Commun.* **2005**, *253*, 118–124.

(13) Ginzburg, P.; Nevet, A.; Berkovitch, N.; Normatov, A.; Lerman, G. M.; Yanai, A.; Levy, U.; Orenstein, M. Plasmonic resonance effects for tandem receiving-transmitting nanoantennas. *Nano Lett.* **2011**, *11*, 220–224.

(14) Zhang, S.; Wei, H.; Bao, K.; Håkanson, U.; Halas, N. J.; Nordlander, P.; Xu, H. Chiral surface plasmon polaritons on metallic nanowires. *Phys. Rev. Lett.* **2011**, *107*, 1–5.

(15) Garoli, D.; Zilio, P.; Gorodetski, Y.; Tantussi, F.; De Angelis, F. Beaming of helical light from plasmonic vortices via adiabatically tapered nanotip. *Nano Lett.* **2016**, *16*, 6636–6643.

(16) Dorn, R.; Quabis, S.; Leuchs, G. Sharper focus for a radially polarized light beam. *Phys. Rev. Lett.* **2003**, *91*, 233901.

(17) Macklin, J. J.; Trautman, J. K.; Harris, T. D.; Brus, L. E. Imaging and time-resolved spectroscopy of single molecules at an interface. *Science* **1996**, *272*, 255–258.

(18) Sick, B.; Hecht, B.; Novotny, L. Orientational imaging of single molecules by annular illumination. *Phys. Rev. Lett.* **2000**, *85*, 4482–4485.

(19) Wong, L. J.; Kärtner, F. X. Direct acceleration of an electron in infinite vacuum by a pulsed radially-polarized laser beam. *Opt. Express* **2010**, *18*, 25035.

(20) Niziev, V. G.; Nesterov, A. V. Influence of beam polarization on laser cutting efficiency. *J. Phys. D. Appl. Phys.* **1999**, *32*, 1455–1461.

(21) Weber, R.; Michalowski, A.; Abdou-Ahmed, M.; Onuseit, V.; Rominger, V.; Kraus, M.; Graf, T. Effects of radial and tangential polarization in laser material processing. *Phys. Procedia* **2011**, *12*, 21–30.

(22) Toyoda, K.; Takahashi, F.; Takizawa, S.; Tokizane, Y.; Miyamoto, K.; Morita, R.; Omatsu, T. Transfer of light helicity to nanostructures. *Phys. Rev. Lett.* **2013**, *110*, 1–5.

(23) Yao, A. M.; Padgett, M. J. Orbital angular momentum: origins, behavior and applications. *Adv. Opt. Photonics* **2011**, *3*, 161–204.

(24) Bliokh, K. Y.; Nori, F. Transverse and longitudinal angular momenta of light. *Phys. Rep.* **2015**, *592*, 1–38.

(25) Aiello, A.; Banzer, P.; Neugebauer, M.; Leuchs, G. From transverse angular momentum to photonic wheels. *Nat. Photonics* **2015**, *9*, 789–795.

(26) Neugebauer, M.; Eismann, J. S.; Bauer, T.; Banzer, P. Magnetic and electric transverse spin density of spatially confined light. *Phys. Rev. X* **2018**, *8*, 21042.

(27) Rodríguez-fortuño, F. J.; Marino, G.; Ginzburg, P.; O'Connor, D.; Martínez, A.; Wurtz, G. A.; Zayats, A. V. Near-field interference for the unidirectional excitation of electromagnetic guided modes. *Science* **2013**, *340*, 328–330.

(28) Bauer, T.; Banzer, P.; Karimi, E.; Orlov, S.; Rubano, A.; Marrucci, L.; Santamato, E.; Boyd, R. W.; Leuchs, G. Observation of optical polarization Möbius strips. *Science* **2015**, *347*, 964–966.

(29) Maucher, F.; Skupin, S.; Gardiner, S. A.; Hughes, I. G. Creating Complex Optical Longitudinal Polarization Structures. *Phys. Rev. Lett.* **2018**, *120*, 163903.

(30) Wan, C.; Zhan, Q. Generation of exotic optical polarization Möbius strips. *Opt. Express* **2019**, *27*, 11516.

(31) Novotny, L.; van Hulst, N. Antennas for light. *Nat. Photonics* **2011**, *5*, 83–90.

(32) Biagioni, P.; Hecht, B.; Huang, J.-s. Nanoantennas for visible and infrared radiation. *Reports Prog. Phys.* **2012**, *75*, 024402.

(33) Guo, Z.; Li, Z.; Zhang, J.; Guo, K.; Shen, F.; Zhou, Q.; Zhou, H. Review of the functions of Archimedes' spiral metallic nanostructures. *Nanomaterials* **2017**, *7*, 405.

(34) Chen, W.; Nelson, R. L.; Zhan, Q. Efficient miniature circular polarization analyzer design using hybrid spiral plasmonic lens. *Opt. Lett.* **2012**, *37*, 1442.

(35) Guo, Q.; Zhang, C.; Hu, X. A spiral plasmonic lens with directional excitation of surface plasmons. *Sci. Rep.* **2016**, *6*, 1–7.

(36) Mao, L.; Ren, Y.; Lu, Y.; Lei, X.; Jiang, K.; Li, K.; Wang, Y.; Cui, C.; Wen, X.; Wang, P. Far-field radially polarized focal spot from plasmonic spiral structure combined with central aperture antenna. *Sci. Rep.* **2016**, *6*, 1–8.

(37) Cheng, L.; Li, X.; Wang, Z.; Cao, P.; He, X.; Niu, T. Adjustable 3D plasmonic Archimedes spiral lens for optical manipulation. *Appl. Sci.* **2019**, *9*, 674.

(38) Rui, G.; Chen, W.; Abeysinghe, D. C.; Nelson, R. L.; Zhan, Q. Beaming circularly polarized photons from quantum dots coupled with plasmonic spiral antenna. *Opt. Express* **2012**, *20*, 19297.

(39) Liu, H.; Mehmood, M. Q.; Huang, K.; Ke, L.; Ye, H.; Genevet, P.; Zhang, M.; Danner, A.; Yeo, S. P.; Qiu, C. Twisted focusing of optical vortices with broadband flat spiral zone plates. *Adv. Opt. Mater.* **2014**, *2*, 1193–1198.

(40) Mehmood, M. Q.; Liu, H.; Huang, K.; Mei, S.; Danner, A.; Luk'yanchuk, B.; Zhang, S.; Teng, J.; Maier, S. A.; Qiu, C. Broadband spin-controlled focusing via logarithmic-spiral nanoslits of varying width. *Laser Photon. Rev.* **2015**, *9*, 674–681.

(41) Bachman, K. A.; Peltzer, J. J.; Flammer, P. D.; Furtak, T. E.; Collins, R. T.; Hollingsworth, R. E. Spiral plasmonic nanoantennas as circular polarization transmission filters. *Opt. Express* **2012**, *20*, 1308–1319.

(42) Schäferling, M.; Yin, X.; Engheta, N.; Giessen, H. Helical plasmonic nanostructures as prototypical chiral near-field sources. *ACS Photonics* **2014**, *1*, 530–537.

(43) Esposito, M.; Tasco, V.; Todisco, F.; Cuscunà, M.; Benedetti, A.; Scuderi, M.; Nicotra, G.; Passaseo, A. Programmable extreme chirality in the visible by helix-shaped metamaterial platform. *Nano Lett.* **2016**, *16*, 5823–5828.

(44) Kosters, D.; De Hoogh, A.; Zeijlemaker, H.; Acar, H.; Rotenberg, N.; Kuipers, L. Core-shell plasmonic nanohelices. *ACS Photonics* **2017**, *4*, 1858–1863.

(45) Woźniak, P.; De Leon, I.; Höflich, K.; Haverkamp, C.; Christiansen, S.; Leuchs, G.; Banzer, P. Chiroptical response of a single plasmonic nanohelix. *Opt. Express* **2018**, *26*, 19275.

(46) Wang, M.; Salut, R.; Suarez, M. A.; Martin, N.; Grosjean, T. Chiroptical transmission through a plasmonic helical traveling-wave nanoantenna, towards on-tip chiroptical probes. *Opt. Lett.* **2019**, *44*, 4861.

(47) Höflich, K.; Feichtner, T.; Hansjürgen, E.; Haverkamp, C.; Kollmann, H.; Lienau, C.; Silies, M. Resonant behavior of a single plasmonic helix. *Optica* **2019**, *6*, 1098.

(48) Kraus, J. D.; Marhefka, R. J.; Khan, A. S. *Antennas and wave propagation*, 4th ed.; Tata McGraw Hill: New York, 2006; p 962.

(49) Gansel, J. K.; Latzel, M.; Frölich, A.; Kaschke, J.; Thiel, M.; Wegener, M. Tapered gold-helix metamaterials as improved circular polarizers. *Appl. Phys. Lett.* **2012**, *100*, 101109–1–101109–3.

(50) Esposito, M.; Tasco, V.; Todisco, F.; Benedetti, A.; Sanvitto, D.; Passaseo, A. Three dimensional chiral metamaterial nanospirals in the visible range by vertically compensated focused ion beam induced-deposition. *Adv. Opt. Mater.* **2014**, *2*, 154–161.

(51) Woźniak, P.; De Leon, I.; Höflich, K.; Leuchs, G.; Banzer, P. Interaction of light carrying orbital angular momentum with a chiral dipolar scatterer. *Optica* **2019**, *6*, 961.

(52) El Beainou, R.; Chargui, A.; Pedrosa, P.; Mosset, A.; Euphrasie, S.; Vairac, P.; Martin, N. Electrical resistivity and elastic wave propagation anisotropy in glancing angle deposited tungsten and gold thin films. *Appl. Surf. Sci.* **2019**, *475*, 606–614.

(53) Bliokh, K. Y.; Rodríguez-Fortuño, F. J.; Nori, F.; Zayats, A. V. Spin-orbit interactions of light. *Nat. Photonics* **2015**, *9*, 796–808.

(54) Gibbs, J. G.; Mark, A. G.; Eslami, S.; Fischer, P. Plasmonic nanohelix metamaterials with tailorable giant circular dichroism. *Appl. Phys. Lett.* **2013**, *103*.

(55) Esposito, M.; Tasco, V.; Cuscunà, M.; Todisco, F.; Benedetti, A.; Tarantini, I.; Giorgi, M. D.; Sanvitto, D.; Passaseo, A. Nanoscale 3D chiral plasmonic helices with circular dichroism at visible frequencies. *ACS Photonics* **2015**, *2*, 105–114.

(56) Chang, D. E.; Sørensen, A. S.; Hemmer, P. R.; Lukin, M. D. Quantum optics with surface plasmons. *Phys. Rev. Lett.* **2006**, *97*, 053002.

(57) Garoli, D.; Zilio, P.; De Angelis, F.; Gorodetski, Y. Helicity locking of chiral light emitted from a plasmonic nanotaper. *Nanoscale* **2017**, *9*, 6965–6969.

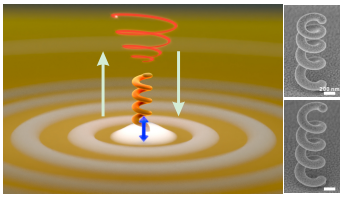

Figure 6: For TOC only